ELSEVIER

Contents lists available at ScienceDirect

Geomechanics for Energy and the Environment

journal homepage: www.elsevier.com/locate/gete



Quantitative assessment of well leakage, part II: Case studies for CCS

Al Moghadam a,* D, Sahar Amiri b

- ^a TNO Energy and Materials Transition, Utrecht, the Netherlands
- ^b Utrecht University, Utrecht, the Netherlands

ARTICLE INFO

Keywords:
Well leakage
CCS
Microannuli
Aquifer storage
Storage pressure
Migration
Self-sealing

ABSTRACT

This paper presents the second part of a two-part series on estimating fluid migration along wells. We use the results of the model described in the first paper and outline a leakage calculation methodology. The present method considers the mechanical behaviour of the flow pathway, formation creep, visco-inertial effects, and the operational conditions of the well to provide a deterministic evaluation of fluid migration along the well. Two case studies are presented that focus on a $\rm CO_2$ injection well in a depleted reservoir and a legacy well in an aquifer CCS project.

The results indicate that there is a pressure threshold below which ${\rm CO_2}$ may not flow through the cemented annulus. Beyond that point, the flow rate increases non-linearly with storage pressure. The size of the leakage pathway changes over time with the pressure and temperature of the system and is not a static parameter. Viscoinertial effects and creep could reduce the potential leak rate. The computed rates should be considered as an upper bound in this work as the impact of multiphase flow was not considered. This type of assessment is critical to conduct quantitative risk assessments for CCS projects. The results enable operators to manage storage pressure, reduce the cost of MMV (Measurement, Monitoring, and Verification) plans, and improve well designs. We argue that the impact of the magnitude of leakage rates reported in this work should be weighed against the improvements to the economics of CCS projects with an increased pressure/storage capacity.

Introduction

Quantitative assessment of well leakage has been gaining attention in recent years. Methane leakage along active and abandoned wells is a source of fugitive methane emissions. 24,46 In addition, investigating fluid migration along injector and legacy wells is of interest for the containment of CO₂ in carbon capture and storage (CCS) projects.³⁵ Well leakage is also an area of interest in nascent technologies such as underground hydrogen storage. Regardless of the context, we need to understand the potential magnitude and the pathways of unwanted fluid migration in order to assess the consequences, monitoring strategies, and potential mitigation technologies. In other words, quantitative assessment of risk requires a reliable estimate of well leakage under the particular operational conditions of a project. This type of assessment is needed for licensing and the project design phase. The results can be used to estimate harmful environmental outcomes, in addition to improving the economics of projects by reducing costly workovers or overly conservative storage pressure limits.

Well leakage is a relatively broad term. The flow path may be

through the cemented annulus, through the casing/tubing joints or body, through well equipment such as packers, through cement plugs in case of plugged & abandoned wells, or a combination of all. 17 In addition to the pathway, the source of leaking fluid may vary significantly. The leaking fluid may originate from the target reservoir, storage formation, or a shallow gas pocket penetrated by the well.³ The consequence of fluid migration may also vary depending on the outlet of the flow and its magnitude. Migrated fluids may accumulate in a deep aquifer, near a well and mainly in a dissolved phase which is relatively benign; or flow into freshwater aquifers and the atmosphere affecting the environment adversely.³¹ Typically, the term "migration" is used when fluids move within the storage system, while the term "leakage" implies fluid movement out of the storage zone. However, the definition of the storage system is not always based on geology but local regulations and legal agreements. In this work, we use these terms interchangeably as we focus on unwanted flow of fluids along wellbores, regardless of the definition of the boundaries of the storage complex.

Intact cement's matrix permeability is sufficiently low to prevent flow along a well. 41 However, there are three main failure modes in

^{*} Correspondence to: TNO Energy and Materials Transition, Princetonlaan 6, 3584 CB, Utrecht, the Netherlands. E-mail address: al.moghadam@tno.nl (A. Moghadam).

cement sheaths that may lead to a pathway for fluid flow. 26 Shear failure, tensile cracking, and debonding from the casing or formation interfaces can occur depending on the particular stress conditions. Shear failure occurs when the deviatoric stress reaches the yield surface. This failure may be ductile or brittle.⁶ Tensile cracks form when the hoop stress in the cement sheath becomes tensile, overcoming the tensile strength of the cement. Typically, this failure occurs when the casing pressure increases beyond a certain limit and depends on the degree of confinement. Shear and tensile cracks are likely not continuous and may not conduct fluids over the length of the cement sheath. 12,43 The debonding of the interface between the cement and the casing or the formation can lead to microannuli. Debonding occurs when the radial stress at the interface becomes tensile and overcomes the hydraulic or normal bond strength of the interface. These open interfaces have a rather long profile equal to the perimeter of the casing or outer cement, much longer than tensile or shear cracks. In addition, they can be continuous along the well with apertures ranging between 5 and 200 μm. ^{14,29} Therefore, microannuli pose a more significant risk to well leakage.

In order to estimate fluid flow rate through microannuli, we need to predict the presence and the aperture of the pathway. Jackson, Murphey conducted experiments on a cement sheath between two casings. Their investigations showed that microannuli can form due to plastic compression of the cement sheath at high casing pressures, which open up as the casing pressure is subsequently lowered. Boukhelifa et al. 8 used a mechanical device to expand and shrink the inner casing of a lab-scale cement sheath. Their results showed that flexible and expanding cement systems performed better during loading and unloading stages. Therond et al. 43 conducted large-scale laboratory experiments to determine the size of the microannuli at various casing pressure and temperature conditions. Their results showed an inner microannuli due to the cooling of the casing. De Andrade et al. 13 used X-Ray computer tomography (CT) to visualize the microannuli and tensile cracks in cement sheaths. Stormont et al. ⁴¹ conducted extensive laboratory tests to characterize the size of microannuli under different casing pressure and confining stress conditions. According to their experiments, microannuli behave similarly to fractures, which means that the normal stress at the interface controls the size and permeability of the opening. Hatambeigi et al. ¹⁹ extended that study to investigate the impact of the fluid pressure on the aperture of a cement fracture. Their results confirmed that the width of the fracture is controlled by the effective stress at the interface, with an effective stress coefficient equal to 1.0. Moghadam et al. ²⁹ also reported pressure and stress-dependent microannuli aperture in a large-scale experimental setup. They reported that hydraulic aperture of the microannuli may be lower than the mechanical aperture. Meng et al. ²⁸ confirmed the pressure dependency of permeability in microannuli. The experimental results in the literature clearly point to a pressure-sensitive microannuli aperture. This means that the equivalent permeability of the cement sheath depends on the effective radial stress at either of the cement interfaces. Therefore, the permeability can change over time (due to the change in pressure and temperature), and over the length of the well (as the pressure of the leaking fluid drops). A constant equivalent permeability assumption is not appropriate for the leakage pathway in wells.

Predicting the state of stress in the cement sheath is required to predict the likelihood and size of microannuli. The state of stress depends on the initial slurry pressure, mechanical properties of the formation, mechanical and hydration properties of cement, and the operational condition of the well (e.g., casing pressure and temperature³⁰;). Staged finite element (FEA) models have been used extensively to track the cement stress from the moment of placement to the end of the well's life. ^{18,34,51,7} The key to the accuracy of such simulations is the consideration of the initial state of stress in cement. ^{30,38,6} The initial state of stress in cement evolves during hydration reactions and the subsequent pore pressure change as the cement sets. ^{1,27} Moghadam and Loizzo ³⁰ presented a methodology to incorporate the impact of

cement's hydration reactions in a staged thermo-hydro-mechanical FEA model to predict the stress evolution in a cement sheath. This methodology can predict the occurrence of the microannuli and its size, verified by lab experiments conducted by Meng et al. ²⁷ However, staged FEA models typically do not consider the impact of the flowing fluid on the size of the microannuli.

There has been extensive well leakage modelling efforts previously done in the literature. ^{31,33,35,36,37,39} These studies use a numerical flow model (typically finite difference or volume) that mimics the near well region. The cement sheath is considered to be the flow pathway with a constant permeability. The cement sheath connects the source of gas to shallow aquifers or the atmosphere. Mass balance equations are solved to estimate the flow of gas through the cement sheath. The general conclusion from such studies is that the cement sheath permeability is the most influential parameter controlling the flow rate. However, cement permeability is an input parameter in all such analyses and does not change over the duration of the simulations. The mechanical behavior of the microannuli with respect to the operational condition of the well cannot be modelled using flow models. Therefore, at best these studies can be used to conduct sensitivity analyses rather than reliable prediction of fluid migration along wells in a particular region.

Geomechanical studies in the literature have improved over time to include the important physical processes needed to estimate the size of the microannuli over the life of the well. Flow models are capable of using appropriate equations of state and flow path to predict the leak rates for a given permeability. However, there is a lack of a methodology that combines geomechanical and flow assessment tools to predict the cement sheath permeability and the leak rate considering the operational parameters of a well. This paper is Part II of a two-part series initially reported by Moghadam and Loizzo.³⁰ The Part I paper focuses on estimating the cement stress evolution during curing which is crucial for the estimation of microannuli formation and its size. This paper aims to couple the geomechanical model with a flow model to estimate gas leakage through microannuli in wells. The significance of this methodology is that the level of cement damage (i.e., cement permeability) is not a model input, but predicted based on the near-well stress evolution. This produces a methodology that can predict well leakage based on a particular well design, formation properties, and operational history. The tool developed in this work is applied to two case studies related to a CCS project in the Dutch North Sea, one pertaining to an injector well and the second to a legacy well.

Methodology

Part I of this work describes the methodology to predict cement's stress evolution considering the impact of cement hydration rate, the evolution of cement's mechanical properties, chemical shrinkage, and the pressure and temperature variation in the well.³⁰ The presence and the size of the microannulus (MA) are derived based on the radial stress and the displacement at the interfaces. The results were verified using lab experiments measuring cement stress during curing.²⁷ The present paper focuses on using the estimated size of the microannulus to calculate the potential fluid flow rate through the cemented annulus of production casing/liner. The presence of a MA does not necessarily lead to fluid migration. A sufficient pressure gradient must also exist for the gas to exit the reservoir or storage complex. The upstream pressure of the gas depends on the injection strategy or source pressure which is an input to the model. The present methodology assumes a simple migration pathway, comprised of a MA connecting the reservoir to the overburden (Fig. 3). The overburden is assumed to have sufficient permeability to receive the entire flow rate with negligible change in its pressure.

We use the results of the staged FEA model described in Part I (in terms of the size of the microannulus) as an input to the leakage calculation. The size of the microannulus along the well is revised based on the estimated flowing pressure to take into account the pressure

dependency of the aperture. The appropriate equations of state are used to calculate the gas viscosity and density at the relevant pressure/temperature conditions. The impact of formation creep on the size of the microannuli is considered over time. Finally, the impact of visco-inertial flow conditions (non-Darcy flow) on the flow rate is also included in the present modelling framework. The details of the methodology are outlined in the following sections.

Pressure dependency

If fluids begin to flow through the MA, the pressure of the fluid may inflate or deflate the MA size. ^{19,28,29} The FEA model calculates the MA size assuming that the fluid pressure is equal to the caprock pressure (effective stress at the open interface is zero). If the pressure of the leaking fluid is different from this value, the size of the MA will change accordingly. Thick cylinder theory can be used to estimate the change in the aperture of the MA based on the change in fluid pressure inside the MA.

A representation of the thick cylinder theory parameters is demonstrated in Fig. 1 (left). Eq. 1 is derived from the thick cylinder theory to estimate the radial displacement in medium "m" at the radius "r".

$$\Delta u_r^m = A_r^m \Delta P_{out} + B_r^m \Delta P_{in} \tag{1}$$

 ΔP_{out} and ΔP_{in} are the changes in stress/pressure on the outside and inside of the cylinder, respectively. Compressive pressure is negative in this formulation. A_r^m and B_r^m are parameters related to the elastic properties and the dimensions of the medium and can be calculated using Eq. 2 and Eq. 3:

$$A_r^m = \frac{2(1-2\nu^m)r_o^2r^2 + r_o^2r_i^2}{2G^m(r_o^2 - r_i^2)r} \tag{2} \label{eq:alpha}$$

$$B_r^m = \frac{-2(1 - 2\nu^m)r_i^2r^2 + r_o^2r_i^2}{2G^m(r_o^2 - r_i^2)r}$$
 (3)

where, ν^m and G^m are the Poisson's ratio and Shear Modulus of the medium m, respectively. r_i and r_o are the inner and outer radius of the medium, respectively.

First, let us consider the case for an inner MA (at the casing/cement interface), as presented in Fig. 1 (right). ΔP_{ma} is the change in the fluid pressure inside the MA due to fluid migration. Variation in MA pressure also changes the stress at the interface of the cement and formation. Using Eq. 1, we can write an expression for the displacement at the outer interface of cement, and the inner interface of the formation, as below:

$$\Delta u_{ro}^{cem} = A_{ro}^{cem} \Delta P_{int} + B_{ro}^{cem} \Delta P_{ma} \tag{4}$$

$$\Delta u_{ri}^f = A_{ri}^f \Delta P_{stress} + B_{ri}^f \Delta P_{int} \tag{5}$$

"f" and "cem" denote formation and cement, respectively. ΔP_{stress} is

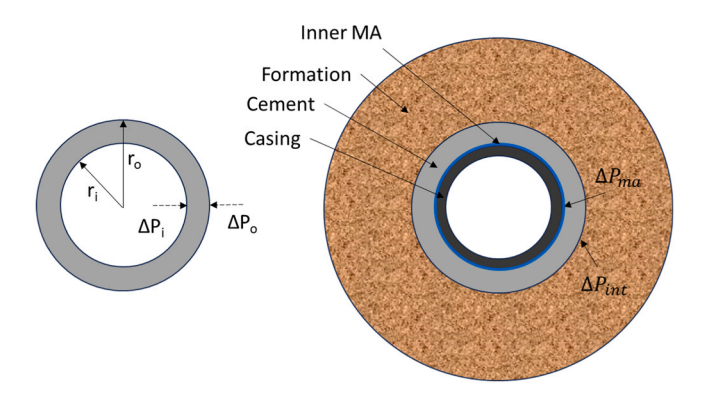


Fig. 1. The idealized schematic of the near well region on the right, and the representation of parameters in Eq. 1, on the left.

the change in the far-field stresses in the formation and can be assumed to be zero (no change in far field stress is expected due to fluid migration). Assuming a bonded interface between the cement and the formation (as only one microannulus can be open at any given time), we can set Eq. 4 and Eq. 5 equal to get:

$$\Delta P_{\rm int} = \frac{B_{\rm re}^{\rm rem} \Delta P_{\rm ma}}{B_{\rm ri}^{\rm f} - A_{\rm rem}^{\rm cem}} \tag{6}$$

Using Eq. 1, we can write the following expressions to calculate the displacement at the outer interface of the casing and inner interface of cement:

$$\Delta u_{ri}^{cem} = A_{ri}^{cem} \Delta P_{int} + B_{ri}^{cem} \Delta P_{ma} \tag{7}$$

$$\Delta u_{ro}^{cas} = B_{ro}^{cas} \Delta P_{ma} \tag{8}$$

The total change in aperture is the sum of the magnitude of the two expressions above (note that the casing displacement is negative and therefore the sign is changed below):

$$\Delta e_h = \Delta u_{ri}^{cem} - \Delta u_{ro}^{cas} \tag{9}$$

A similar exercise for the outer MA yields the following equations to calculate the change in the MA aperture with a change in fluid pressure:

$$\Delta P_{\rm int} = \frac{A_{ri}^{cem} \Delta P_{ma}}{A_{ros}^{cos} - B_{ri}^{cem}} \tag{10}$$

$$\Delta u_{ri}^f = B_{ri}^f \Delta P_{ma} \tag{11}$$

$$\Delta u_{ro}^{cem} = A_{ro}^{cem} \Delta P_{ma} + B_{ro}^{cem} \Delta P_{int} \tag{12}$$

$$\Delta e_h = \Delta u_{ri}^f - \Delta u_{ro}^{cem} \tag{13}$$

The derivations above are used in the leakage calculation methodology to estimate the inflation/deflation level of the MA due to fluid pressure changes.

Creep

Certain materials such as salt and shale formations undergo time-dependent displacements when exposed to deviatoric stress. In some cases, casing collapse has been attributed to excessive levels of creep under high stress conditions. ⁴² Upon drilling the well, the stress equilibrium in the near-well vicinity is disturbed and the formation is exposed to deviatoric stress. If the formation is prone to creep, it moves towards the well at a particular rate to reach stress equilibrium again. If an open MA is present, the displacement can potentially close it. This has been proposed as a mechanism to simplify P&A operations when creeping formations are present. ⁴⁵ In the absence of a MA, the radial stress applied by the formation on the cement sheath increases over time

In this work, we calculate the steady-state creep rate using the Double Mechanism (DM) creep law presented as Eq. 14¹⁵:

$$\dot{\varepsilon}_{ss} = \dot{\varepsilon}_0 \exp(\frac{Q}{RT_0} - \frac{Q}{RT}) (\frac{\sigma_d}{\sigma_0})^{n_i}$$
(14)

Where, \dot{e}_0 , σ_0 , and T_0 are the strain rate, deviatoric stress, and temperature at the reference condition, respectively. These parameters are related to the transition of creep mechanism observed in the laboratory. n is the exponent determined from lab experiments. The subscript i refers to the active creep mechanism, namely dislocation creep (n_1) and steady-state cracking (n_2) . Q is the thermal activation energy, R is the universal gas constant, σ_d is the deviatoric stress, and T is the temperature. Eq. 14 is implemented in the Abaqus FEA model using a Fortran subroutine. This allows for the determination of the impact of creep on near-well stresses and MA size. Table 1 presents the input parameters for Eq. 14 used in this work. The data is based on experimental

Table 1Summary of creep parameters used in this work based on. ¹⁵.

Parameter	Unit	Value
$\dot{arepsilon}_0$	s^{-1}	5.239×10^{-9}
σ_0	MPa	9.91
T_0	K	359.15
n_1	[-]	3.36 (if $\sigma_d < \sigma_0$)
n_2	[-]	7.55 (if $\sigma_d > \sigma_0$)
Q	J/mol	50160

measurements reported by Firme et al. 16 and Firme et al. 15 on Brazilian halite. The choice of these values is for demonstration purposes only. The creep parameters should be calibrated with experimental data for the particular caprock of interest.

Finite difference approach

The staged FEA model described in Part I estimates the size of the microannulus (MA) at the center of the caprock, at either the casing or formation interface. If stress anisotropy is present, the size of the MA at a specific depth will not be uniform around the well (in the tangential direction). We take an average of the MA size in the tangential direction to account for the fluctuations around the well. The average aperture change over time is then used for the rest of the calculations. Eq. 15 presents the averaging scheme for the aperture:

$$\overline{e}(\theta) = \sqrt[3]{\frac{1}{2\pi} \int_0^{2\pi} e^3(\theta) d\theta}$$
 (15)

where, \overline{e} is the equivalent aperture, θ is the tangential axis value in the cylindrical coordinate around the well, and e is the aperture at a given θ . The average aperture is based on the equivalent aperture that yields the same flow rate using the cubic law (presented in Eq. 16). Fig. 2 presents a schematic of the non-uniform aperture around the well.

Steady-state flow through a fracture-like MA can be described using Eq. 16, which is a form of the cubic law:

$$\dot{m} = \frac{\rho}{\mu} \times \frac{\pi e_h^3 R}{6} \frac{\partial (P - \rho gz)}{\partial z}$$
 (16)

where, \dot{m} is the mass flow rate of gas, ρ and μ are gas density and viscosity, R is the radius of the MA (either the cement's inner or outer radius), e_h is the hydraulic aperture of the MA, P is the gas pressure, and z represents depth. Eq. 16 considers the impact of buoyancy, which is significant in the case of gas flow. Other assumptions in Eq. 16 include single phase fluid and laminar flow regime. The CoolProp Python library was used to calculate CO₂ density and viscosity as a function of pressure

and temperature (5 ; www.coolprop.org). CoolProp uses the equation of state by Span and Wagner 40 for density calculations and the correlation by Laesecke and Muzny 25 to estimate CO₂ viscosity.

The pressure at the base of the MA is equal to the formation pressure at the base of the caprock in the immediate vicinity of the wellbore. For simplicity, this is assumed to be equal to the bottomhole injection pressure in this work. However, this assumption can be refined by reservoir simulation results. At each time increment, the staged FEA model in Part I calculates the size of the MA according to the injection schedule. Gas density and viscosity are strong functions of pressure and temperature. This complexity hinders a straightforward solution to Eq. 16. We calculated the flow rate in Eq. 16 numerically, using an iterative finite difference procedure similar to Hongjun et al. ²¹

For each timestep, the length of the MA is divided into spatial increments, as demonstrated in Fig. 3. For the first spatial increment, the pressure at the base is known (the injection pressure, which is an input). An initial mass flow rate guess is made using Eq. 16 along the entire path using the average aperture from Eq. 15. Gas density and viscosity are calculated at the pressure and temperature at the base of the element. In addition, the hydraulic aperture is updated according to the upstream pressure using Eq. 2 to Eq. 13. The mass rate guess and the updated parameters are used in Eq. 16 to estimate the pressure at the top of the increment. A similar calculation is done for the subsequent increments until the pressure at the top of the caprock is calculated. This pressure is then compared to the overburden pressure (assumed hydrostatic) to check for convergence. The Newton-Raphson method is used to calculate the next guess for the mass rate until convergence is achieved. Fig. 4 presents a flowchart describing the iterative solution employed in this work to estimate the flow rate along a MA.

Visco-inertial effects

High velocity gas flow through fractures can lead to an excess pressure drop due to visco-inertial effects. ^{11,20,50,52,53} Darcy's flow equation (Eq. 16) describes viscous flow using a linear relationship between the flow rate and the pressure gradient. The visco-inertial flow, also referred to as non-Darcy flow, is typically described using the Forchheimer equation which relates the pressure gradient (or the gradient of the flow potential when considering buoyancy) to flow rate using a quadratic equation. A form of this equation is described in Eq. 17:

$$\frac{\partial (P - \rho gz)}{\partial z} = Aq + Bq^2 \tag{17}$$

where, q is the flow rate and $\frac{\partial (P-\rho gz)}{\partial z}$ is the flow potential gradient. A is the parameter describing pressure drop due to viscous flow, related to permeability and fluid viscosity (Eq. 16). B is a parameter related to

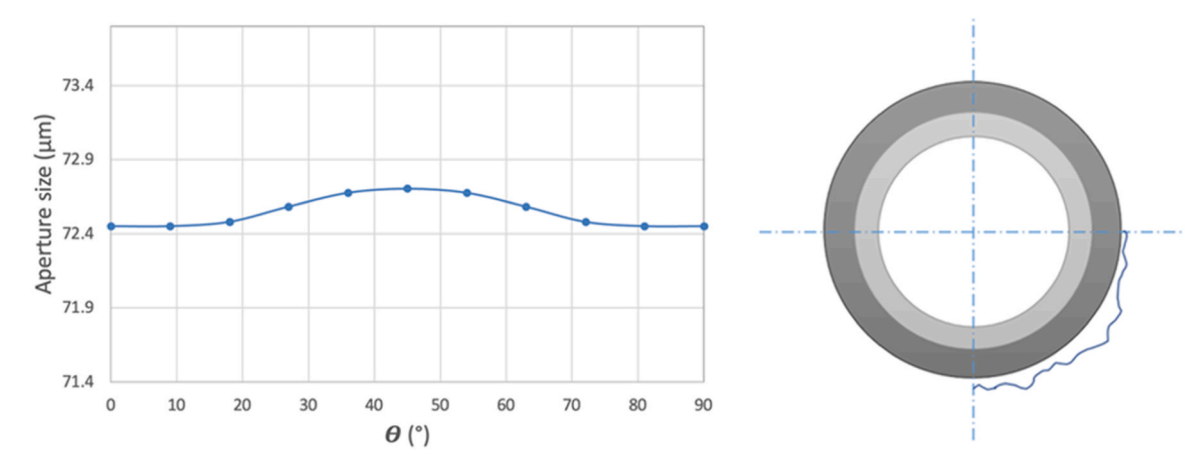


Fig. 2. On the left, an example of the circular distribution of microannulus aperture at one specific depth and time frame from the staged FEA model. On the right, A schematic representation of the possibility of circular non-uniformity of the microannulus aperture around the borehole.

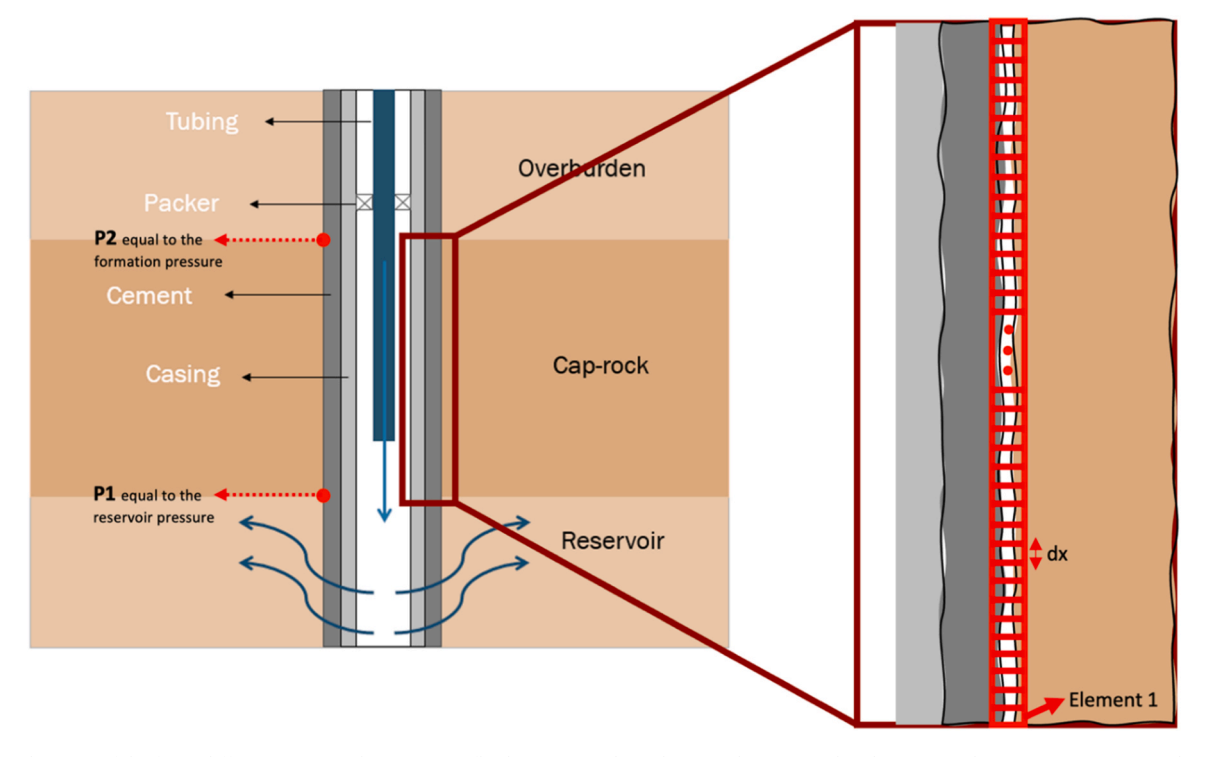


Fig. 3. The schematic of the finite difference approach to estimate fluid migration along the MA. The cement sheath is assumed to contain a microannulus connecting the reservoir to the overburden.

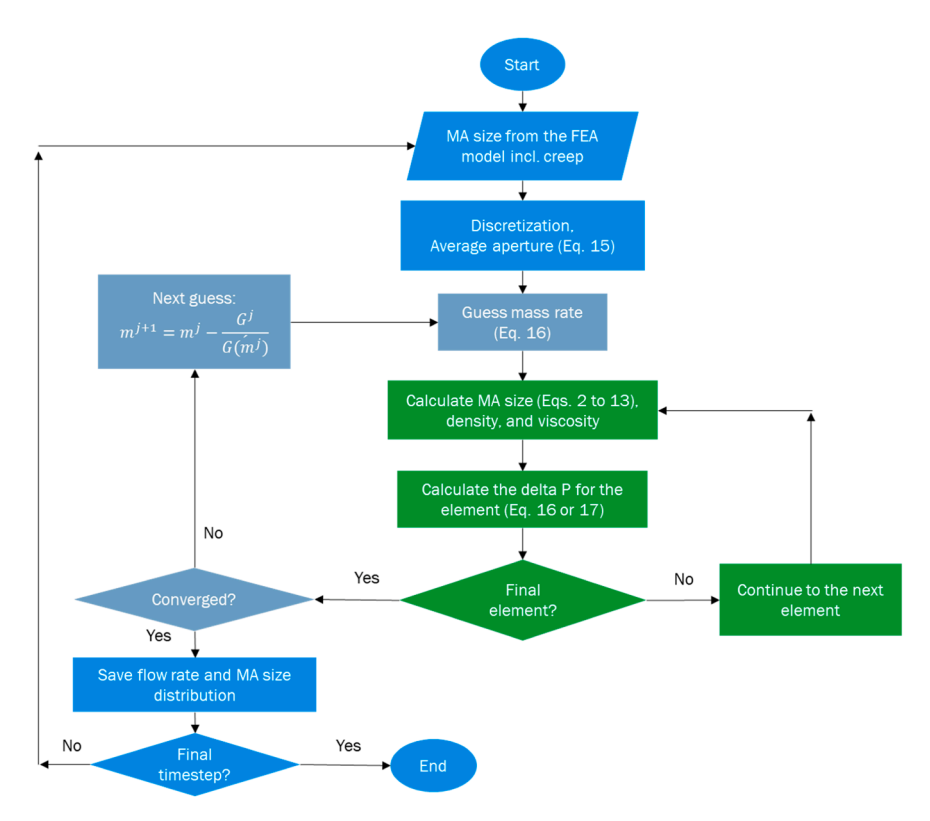


Fig. 4. The flowchart of the iterative finite difference methodology to estimate fluid flow rate along the MA. The colors represent three different loops.

inertial pressure losses. At lower velocities, the second term on the right-hand side of the Eq. 17 becomes negligible. Hatambeigi et al. 20 investigated the visco-inertial flow regime in a fracture in a cement plug. Their results confirm that inertial effects may be significant for gas flow in cement fractures. Chen et al. 11 measured the inertial coefficient B for

several fracture sizes. They proposed a simple correlation as shown in Eq. 18:

$$B = \lambda e_h^{-m} \tag{18}$$

where e_h is the hydraulic aperture and λ and m are empirical coefficients.

Based on the experimental data from Hatambeigi et al. 20 and Chen et al., 11 we assume λ and m to be equal to 10^{24} and 4.5, respectively. If visco-inertial effects are considered, then the pressure drop across an element (Fig. 3) is calculated using Eq. 17. λ and m values assumed here were measured for rough-walled fractures. We assume that these values are also applicable to relatively smoother microannuli.

Self-sealing

Dissolved CO2 in brine can react with cement to form Calcium Carbonate. 10 Previous experimental investigations have shown that under certain conditions, calcium carbonate precipitation can plug fractures and prevent fluid flow. ^{32,47,49} This process is referred to as self-sealing or self-healing of cement fractures. The self-sealing behavior depends on the exposure duration of the dissolved CO2 and cement, and the hydraulic aperture of the MA. The exposure time is typically represented by the residence time, defined as the volume of the fracture (i.e., microannuli) divided by the volumetric flow rate of water through the fracture/MA. The experimental investigations in the literature show that if the velocity of the saturated brine and the size of the pathway are sufficiently small, then the calcite precipitation can plug the path. Nguyen et al., ³² presented a plot of residence time versus hydraulic aperture, identifying three regions for self-sealing, limited sealing, and non-sealing conditions. Wolterbeek et al. 48 updated the plot with a more comprehensive set of experimental results as presented in Fig. 5.

According to Fig. 5, if the residence time and hydraulic aperture combination of the leakage pathway lies in the green region of the plot, the pathway will self-seal. Similarly, the orange region indicates the non-sealing region of the plot. The gray region indicates limited sealing based on the experimental results.

We investigated the potential range of values of residence time of brine in the MA in this study. We used the correlation proposed by Brunet et al. 9 to estimate the self-sealing region boundaries as presented in Eq. 19. Additionally, we used the Iyer et al., 22 model to estimate the residence time below which the CO₂ and cement interaction becomes non-sealing, presented as Eq. 20. τ_c in Eq. 19 and Eq. 20 refers to the residence time in seconds. In order to assess the potential for self-sealing, we calculate the residence time after convergence is reached. The

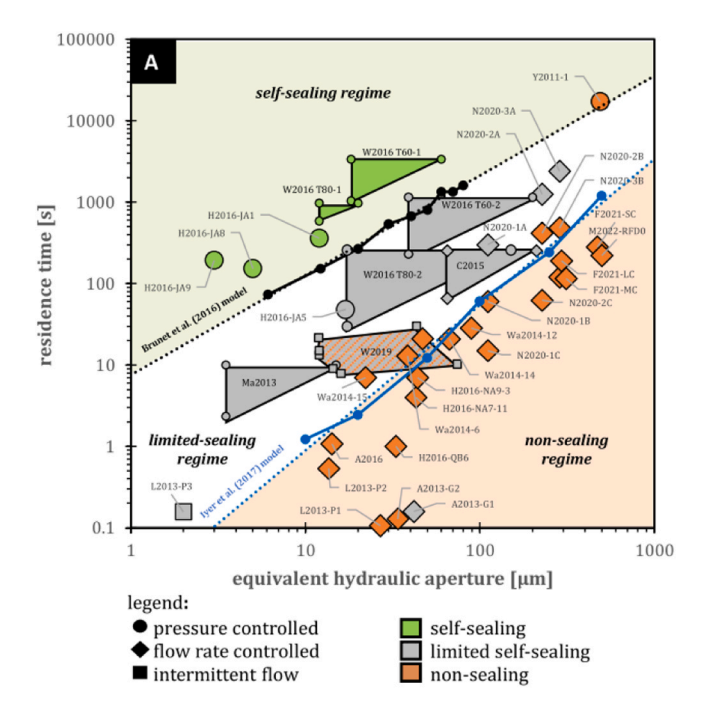


Fig. 5. self-sealing, limited sealing, and non-sealing regions according to the residence time and hydraulic aperture of the fracture. 49 .

residence time is estimated by calculating the hypothetical water flow rate using Eq. 16, and the total volume of the MA (considering the variation of hydraulic aperture along the MA). We used the smallest value of the MA aperture along its length to identify the sealing region using Eq. 19 and Eq. 20. This assumption is due to the fact that the narrowest region in the MA gets plugged first.

$$\tau_c = 9.8 \times 10^{-4} (e_h)^2 + 0.254 (e_h) \tag{19}$$

$$\tau_c = 9.0 \times 10^{-5} (e_h)^2 - 0.0072 (e_h) + 0.2792 \tag{20}$$

Case studies

We used the presented methodology to evaluate the potential fluid migration rate along the cemented annulus for two CCS case studies. The first case study covers an injector well in a depleted gas reservoir. The second case study is related to a legacy well in an aquifer storage project. Both wells are based on typical well designs encountered in the Dutch North Sea. We outline the details of each case study in the following sections.

Depleted gas reservoir storage

This case assumes the reuse of a gas well as a CO2 injection well. A 7" liner is assumed to be cemented across a shale caprock. The well integrity analysis is conducted in the middle of the caprock. The top of the reservoir is assumed to be at a depth of 2500 m, overlain by a 100 m thick caprock. Initially, the well is used for gas production for 10 years. During this time, the reservoir pressure drops from an initial value of 274–50 bar. The bottomhole temperature remains constant at 85 $^{\circ}\text{C}$ during the depletion stage. CO2 injection follows for 12 years, which increases the pressure to 240 bar for the base case, and 274 bar (initial pressure) for the high-pressure case. The temperature of the injected CO₂ at the bottom of the well is assumed to be 15 °C initially, gradually increasing to 35 °C as the pressure increases. The operational parameters are selected based on wellbore and reservoir simulations conducted as part of the ERA ACT RETURN project (www.return-act.eu). After the injection period is over, we continue the calculations for a 5-year period. During the post-injection period, the CO₂ pressure near the well increases by 2 bar due to the gradual heating of the reservoir. CO2 is assumed to be the flowing fluid as the near well region is assumed to be at irreducible water saturation.

Fig. 6 presents the casing pressure and temperature of the well throughout the production, injection and post-injection periods. The temperature during the post-injection period is not prescribed but calculated using a heat transfer analysis. Therefore, the temperature in Fig. 6 does not continue to the end of the simulation time. A comprehensive list of all the parameters used for the case study is provided in Table 2. Table 3 presents the various scenarios that were investigated for each case study.

Aquifer storage

This case considers a legacy well penetrating an aquifer that is used as a CO_2 storage site. A 7" liner is assumed to be cemented across a salt caprock (Zechstein formation). The top of the aquifer is assumed to be at a depth of 3600 m overlain by a 400 m thick caprock. The well was intended as an exploration well and was plugged and abandoned immediately after drilling. CO_2 is assumed to be injected from a nearby location with the plume reaching the well after 2 years. The bottomhole pressure is assumed to linearly increase from 400 to 550 bar over 5 years for the base case. Reservoir temperature is assumed to be constant at 120 °C during the entire operation. Similar to the depleted gas case, we consider a 5-year post-injection period to extrapolate the flow rate into the future. Fig. 7 presents the casing pressure of the well throughout the injection and post-injection periods. A comprehensive list of all the

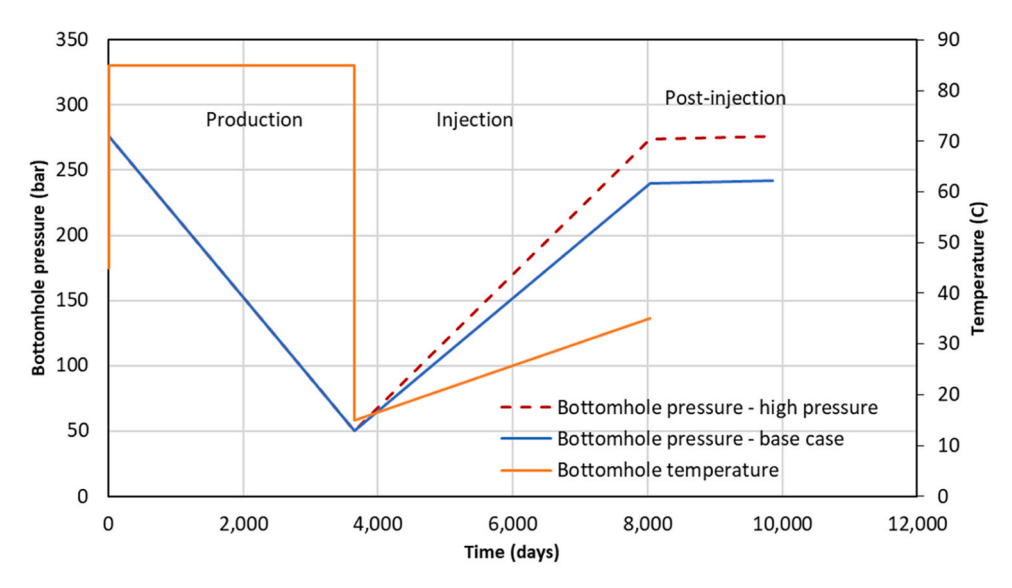


Fig. 6. Casing pressure and temperature during the well's lifetime for the depleted gas case study.

Table 2Summary of all the parameters used for the case study.

Parameter	Unit	Depleted case	Aquifer case
Formation data			
Type Cap rock		Shale	Salt
Thickness caprock	m	100	400
Reservoir top	m	2500	3600
Initial reservoir/aquifer pressure	bar	274	400
Abandonment pressure	bar	50	-
Caprock pressure	bar	274	-
Caprock initial temperature	°C	85	120
Initial stress ratio	[-]	0.63	1.0
Density	kg/m ³	2200	2600
Young's modulus	GPa	16	50
Poisson's ratio	[-]	0.3	0.35
Linear thermal expansion coefficient	K^{-1}	1E-05	1e-5
Heat capacity	J/kg K	887	2000
Thermal conductivity	W/mK	1.4	3.2
Well and cement data			
Hole diameter	m	0.2142	0.2159
Casing/liner OD	m	0.1778	0.1778
Casing/liner ID	m	0.1548	0.1525
Top of Cement	m	2000	3086
Casing shoe depth	m	2550	3623
Well azimuth	deg	0	0
Well inclination	deg	0	0
Mud SG	[-]	1.3	1.65
Cement SG	[-]	1.9	1.95
Young's modulus	GPa	0.1-8	0.1-8
Poisson's ratio	[-]	0.15	0.15
M (critical state model)	[-]	1.50E + 00	1.50E + 00
Pc ₀ (critical state model)	MPa	23	23
λ (critical state model)	[-]	0.02	0.02
κ (critical state model)	[-]	0.0046	0.0046
Thermal conductivity	W/m2K	0.9	0.9
Linear thermal expansion coefficient	K^{-1}	1.30E-05	1.30E-05
Heat capacity	J/kg K	1600	1600

Table 3Summary of the simulation scenarios conducted for each case study.

Parameter	Depleted reservoir case	Aquifer case
Final storage pressure (bar)	240 (base case), 250, 255, 265 274 (initial pressure, high-pressure case)	450, 500, 550 (base case), 600
Impact of creep	✓	✓
Impact of visco- inertial flow	1	✓
Brine flow	×	✓

parameters used for the case study is provided in Table 2.

In some cases, the distance between the legacy well and the injection well is long enough that the CO_2 plume will never reach the legacy well. However, the pressure front may still transmit through brine. Therefore, we also considered the case where the migrating fluid is brine (assuming the same pressure as the CO_2). In addition, due to the presence of brine in the near-well region in this case study, we consider the potential for self-sealing conditions of the MA.

Results

This section presents the results of the flow calculations for each case study using the presented methodology.

Depleted gas reservoir storage case

Fig. 8 presents the evolution of cement temperature, bottomhole injection pressure, and the MA size for the base case (final pressure of 240 bar). The results show an initial MA size of approximately 225 μm after curing. The initial opening of the MA is largely due to the formation pressure, hydration reactions, and the subsequent bulk shrinkage of cement. During depletion, the drop in the reservoir pressure leads to a drop in the MA pressure as well. This deflates the MA aperture and eventually leads to its closure. The temperature remains constant during this phase.

As the cold CO_2 is injected, the temperature of the near-well region drops significantly. The MA does not open immediately after the start of the injection due to high radial stresses caused by the depleted MA. However, the MA eventually opens as the pressure of the reservoir increases. The MA aperture is inflated as the pressure increases until the end of injection. According to Fig. 8, the aperture reaches a high of 220 μm . During the post-injection, the temperature of the near-well region rebounds. This causes a partial closure of the MA down to 140 μm after 5 years.

Despite an open MA, the pressure of the formation remains below the necessary magnitude for CO₂ to migrate out of the storage reservoir and into the overburden. This pressure is determined considering the pressure of the overburden, buoyancy, and assuming a simple pathway. Therefore, the base case does not show CO₂ flowing out of the storage reservoir along the cemented annulus. The base case assumes a maximum injection pressure of 240 bar which is below the hydrostatic pressure at 2500 m. Leakage may still occur inside the casing through plugs, packers, hangers, etc. at pressures below hydrostatic. However,

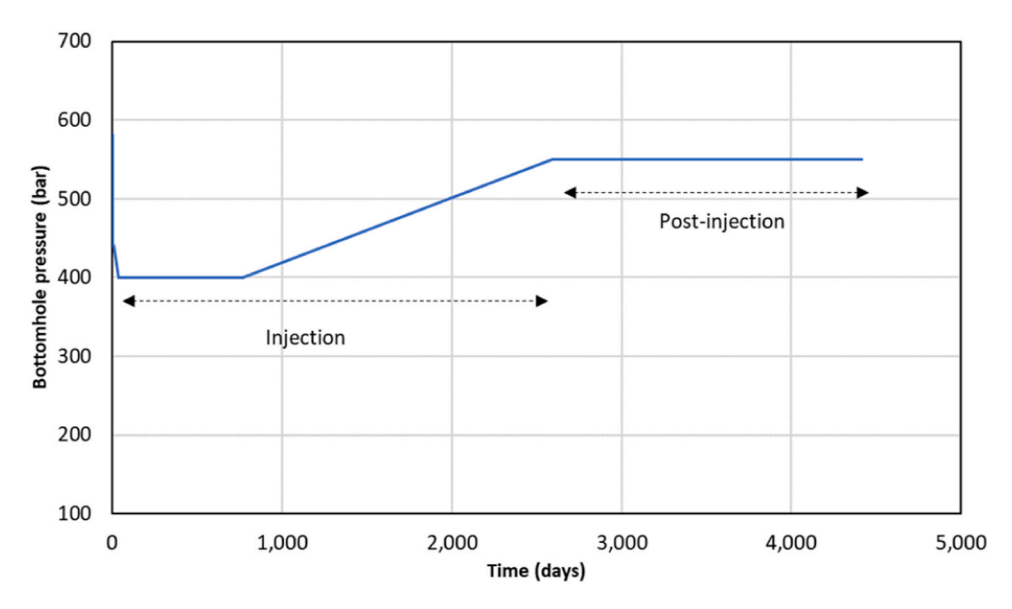


Fig. 7. Casing pressure and temperature during the well's lifetime for the aquifer case study.

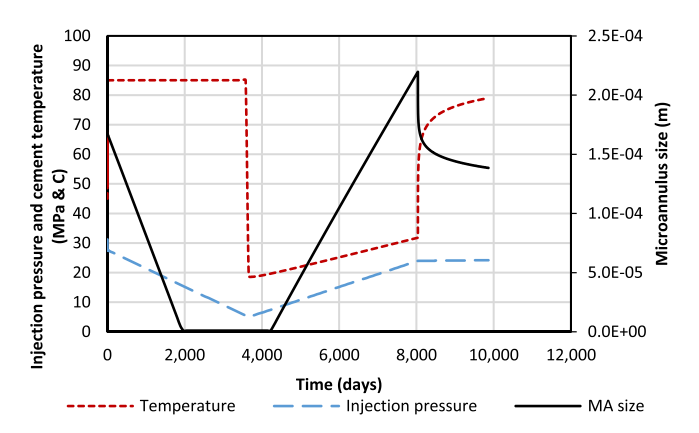


Fig. 8. Evolution of injection pressure, cement sheath temperature, and MA size over time for the depleted gas reservoir storage base case.

this was not considered in this study.

In this case study, we also consider a scenario where the storage pressure is raised to the initial reservoir pressure of 274 bar. This pressure is expected to be safe in terms of caprock integrity and fault reactivation as the system has been under equilibrium with that pressure over geological time. However, the magnitude of fluid migration along

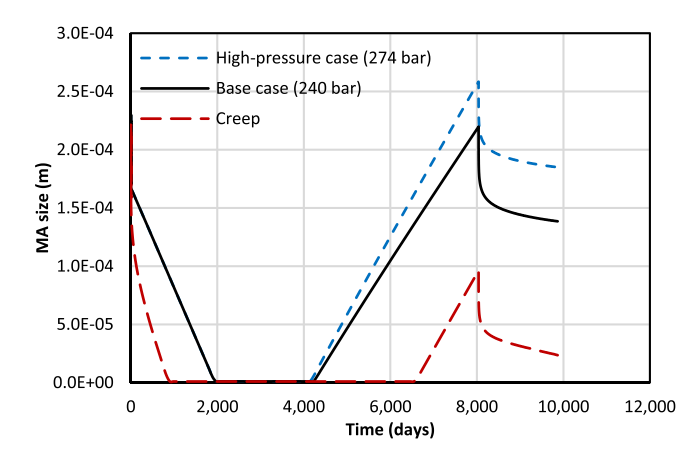


Fig. 9. Evolution of MA size over time for the base case and high-pressure case for the depleted gas field.

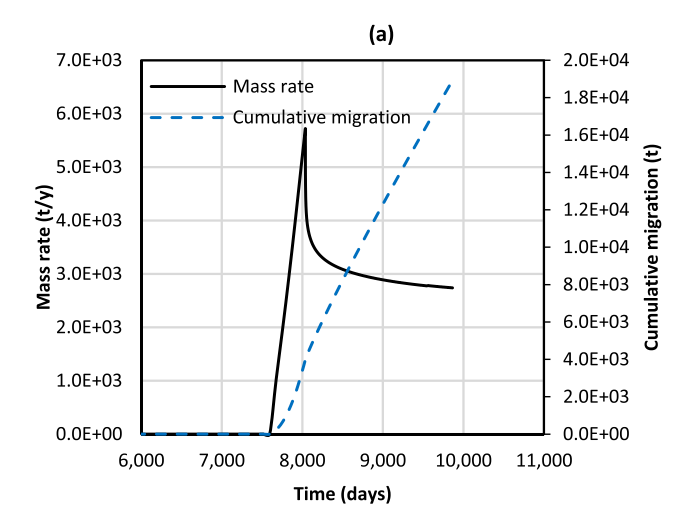
the well should be investigated. Fig. 9 compares the size of the MA over time for several cases. The higher final pressure over the same injection period leads to a larger MA size for the high-pressure case. The MA opens to 260 μm compared to 220 for the base case. The difference is retained during the post-injection period.

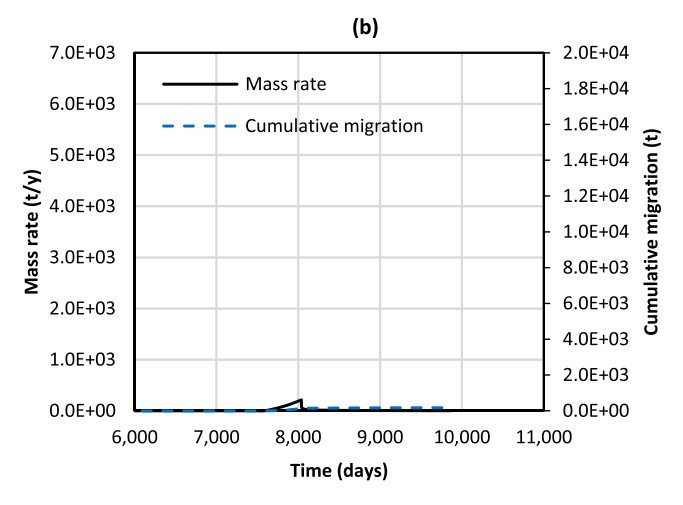
Fig. 10a illustrates the mass rate and cumulative migration of $\rm CO_2$ into the overburden for the high-pressure case. $\rm CO_2$ only begins to flow upwards after the pressure at the top of the reservoir reaches 250 bar. The mass rate increases with the injection pressure to a maximum of 5700 t/y at the end of the injection period. The increase in the mass rate is due to the increase in pressure and to the inflation of the size of the MA. During the post-injection period, the rate drops to 2700 t/y as the MA size decreases due to the temperature rebound. During this time-frame, a total of 18,000 t of $\rm CO_2$ may migrate along the well into the overburden. This is assuming no leak repair tools are used to stop the flow

We investigate the impact of formation creep on the size of the MA and the resulting flow rate. The creep scenario assumes a final storage pressure of 274 bar, similar to the high-pressure case. Fig. 9 illustrates the impact of formation creep on the size of the MA over time. The creep case shows a faster decline in the MA size during the early depletion period. As the MA closes, creep still continues which applies a higher radial stress on the cement sheath. Once injection begins, it takes longer and a higher injection pressure to overcome the radial stress on the cement sheath and reopen the MA. Subsequently, the MA opens to 100 μm at the end of injection, compared to 260 μm for the high-pressure case. During the post-injection period, the MA size decreases to 25 μm due to creep and a temperature rebound (which in turn increases the rate of creep as well). It is possible that over a longer period of time, creep can close the MA altogether.

The smaller MA opening reduces the mass rate and total volume through the cement sheath, as presented in Fig. 10b. The rate increases to 200 t/y at the end of the injection period. During the post-injection period, the rate drops to 2 t/y. In total, 180 t of $\rm CO_2$ may migrate along the well during the simulation period, a factor of 100 times smaller than the high-pressure case.

Including the visco-inertial effects does not change the expected size of the MA as the fluid pressure remains largely the same. However, this effect reduces the gas flow rate due to energy losses from inertial dissipation. Fig. $10 \, \mathrm{c}$ presents the mass rate and cumulative migration values expected for the visco-inertial case with a final storage pressure of 274 bar. The rate increases to $900 \, \mathrm{t/y}$ at the end of injection and declines to $350 \, \mathrm{t/y}$, at the end of the post-injection period. A total of $2700 \, \mathrm{t}$ of





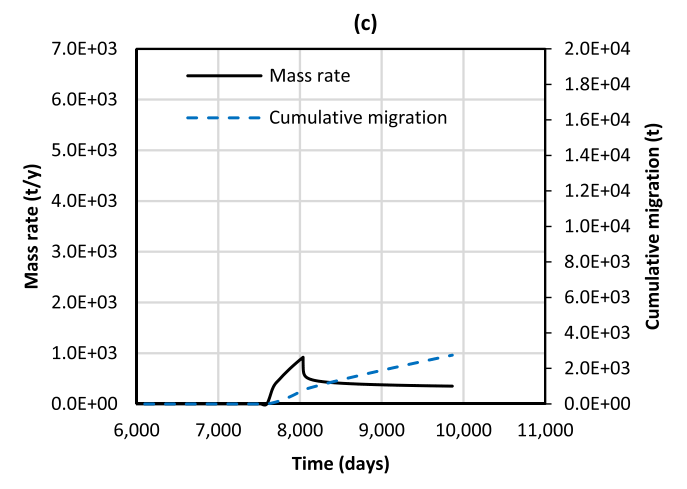


Fig. 10. Mass rate and cumulative migration of CO_2 for the depleted gas reservoir case study. Figure (a) shows the CO_2 rate for the high-pressure case, (b) shows the rate for the creep case, and (c) shows the results for the visco-inertial case. The base case did not show any leakage and therefore not presented here.

CO₂ may migrate along the well by the end of the simulation time.

Aquifer storage case

Fig. 11 shows the bottomhole pressure and the size of the MA for the aquifer storage case. The results for both the base case and the creep

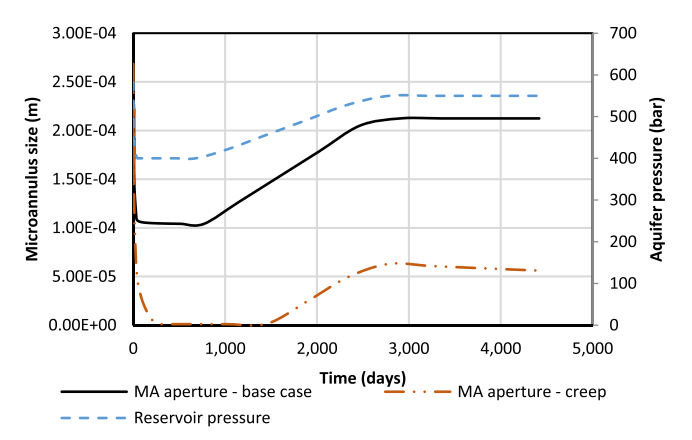


Fig. 11. Evolution of injection pressure and MA size over time for the aquifer storage base case.

scenario are presented in the same figure. An initial MA is observed to be present after the abandonment of the well. During the initial two years, the aquifer pressure and the size of the MA remain constant at 400 bar and 100 μm , respectively. As the high-pressure plume reaches the well, the MA begins to inflate. The temperature is assumed to remain constant and equal to the formation temperature, indicating that the temperature front does not reach the legacy well. The base case sees the plume pressure increase to 550 bar (150 bar over-pressure), which increases the MA size to 210 μm . The pressure and size of the MA are expected to remain constant after the injection stops for the base case.

If formation creep is considered, the initial MA is expected to close gradually. As the plume pressure reaches the well, it first has to overcome the radial stress exerted by the formation creep. Therefore, it takes longer for the MA to open up. The MA size opens to 63 μm by the end of the pressure increase period. As the pressure stabilizes, the MA closes to 56 μm after 5 years.

Fig. 12a presents the mass rates and cumulative CO_2 migration for the base case (550 bar storage pressure). According to Fig. 12a, CO_2 rate reaches an equilibrium value of 2000 t/y during the post-injection period. Fig. 12b presents the fluid migration rate assuming a brine plume. An equilibrium rate of 660 t/y of brine is expected during the post-injection period. This is equivalent to 1.8 m³/d of brine migrating out of the storage reservoir. Fig. 12c presents the results for the creep case which shows an equilibrium mass rate of 2–5 t/y. Fig. 12d presents the same results for the visco-inertial case, indicating an equilibrium mass rate of 300 t/y.

Fig. 13 presents the residence time of saturate brine in the MA after the start of fluid migration for the aquifer storage case. The residence time gradually decreases as the migration rate increases due to the gradual rise in storage pressure. During the post-injection period, residence time remains relatively constant. The residence time resides in the sealing region throughout the simulation time. Therefore, it is plausible that calcite precipitation plugs the pathway and prevents further fluid migration along the well.

Discussion

Migration rate versus storage pressure

Depleted gas reservoir case

Fig. 8, Fig. 9, and Fig. 11 show the evolution of the size of the MA during the wells' operational history. These results demonstrate the dynamic nature of MA as its aperture can vary considerably due to pressure and temperature changes in the well. This indicates that a constant permeability assumption for the cement sheath is not physically meaningful and leads to significant errors in estimating migration rates over time. The present analysis can be repeated at several depths

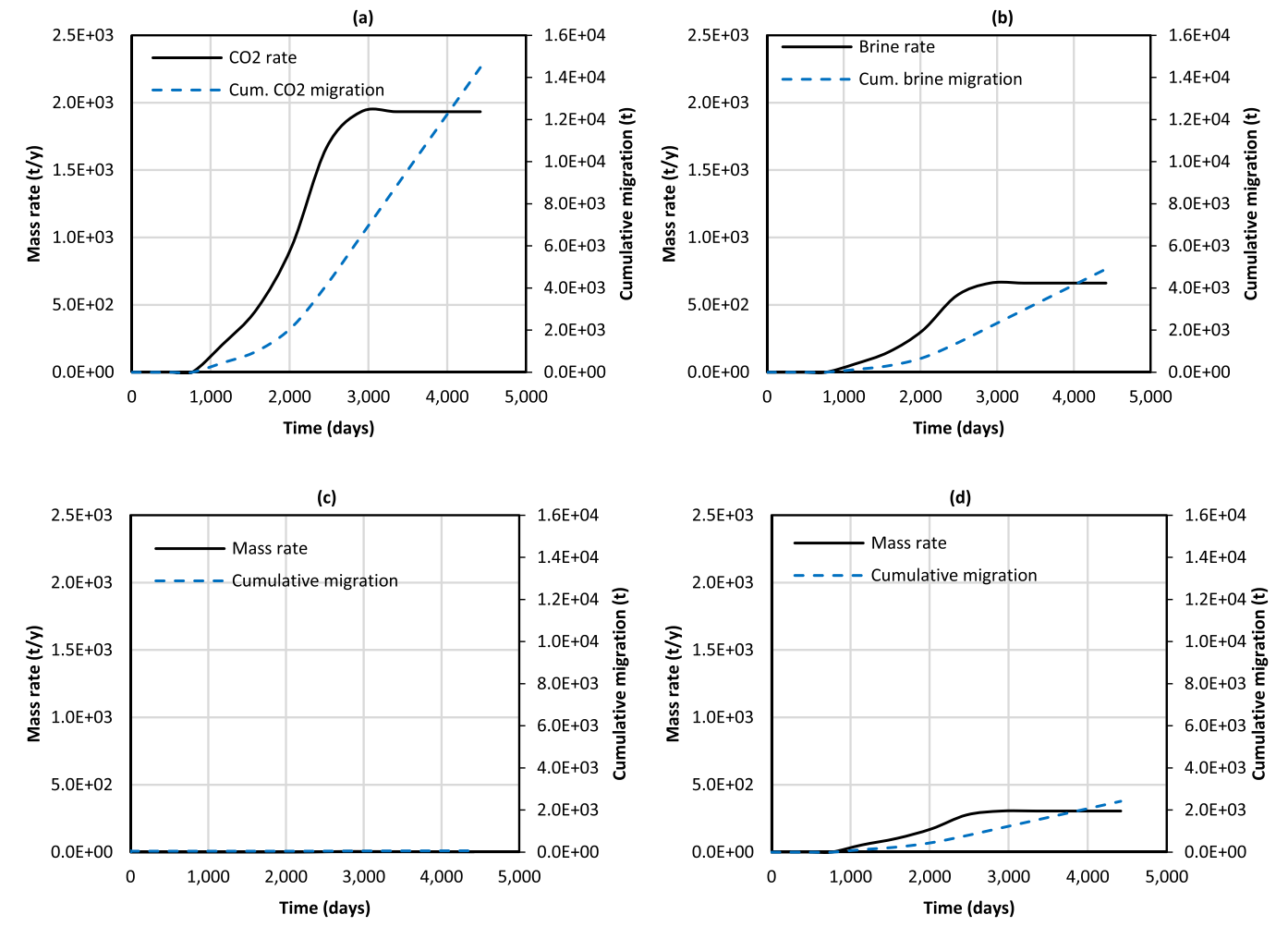


Fig. 12. Mass rate and cumulative migration of fluids for the aquifer storage case study (550 bar storage pressure). Figure (a) illustrates CO_2 rate for the base case, (b) shows the brine rate for the base case, (c) shows the CO_2 rate for the creep case, and (d) shows the CO_2 rate for the visco-inertial case.

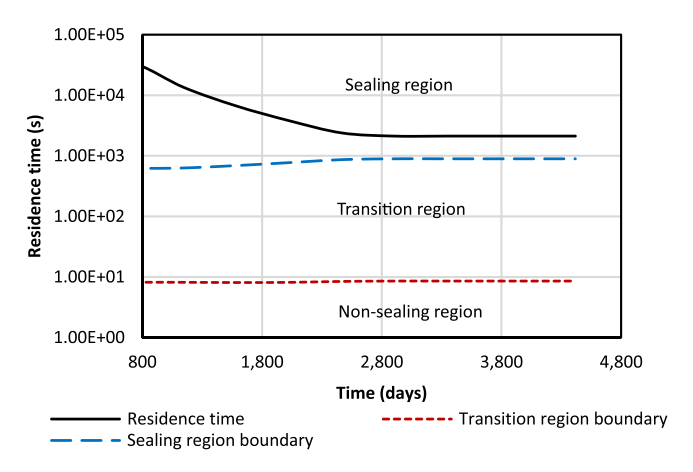


Fig. 13. Residence time of dissolved CO_2 in the MA with respect to the sealing and transition regions for the aquifer storage case.

along the well to investigate the dynamic size of the MA along the well for different casing strings. The input parameters in the present case studies are relatively representative of the Dutch North Sea wells. However, this does not imply that MAs are necessarily present in all wells. The model calculates the stresses and displacements at the cement interfaces to evaluate whether MA forms. Formation mechanical properties, slurry density, and the length of the cement sheath are the critical

parameters that control the formation and size of the MA. A more comprehensive discussion on this is provided in the Part I of this paper.³⁰

Fig. 14 presents the CO_2 migration rate over time for several scenarios related to the depleted gas reservoir storage case study. CO_2 only begins flowing (outside the casing) after the pressure at the reservoir top reaches 250 bar. For the base case, the maximum pressure is limited to 240 bar. Therefore, despite the presence of a pathway, no migration is expected. In fact, brine may flow from the overburden into the reservoir.

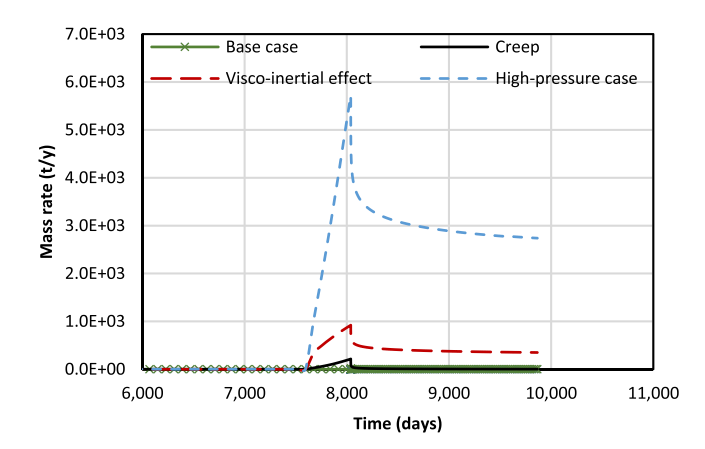


Fig. 14. Comparison of the ${\rm CO_2}$ mass rates considering different scenarios for the depleted reservoir storage case.

The high-pressure case sees reservoir pressure as high as 274 bar. This leads to a max rate of $5700\,t/y$ of CO_2 at the end of the injection period. Including visco-inertial effects reduces the max rate to $900\,t/y$. If the creep rate of the formation is considered, the maximum rate drops to $200\,t/y$. The combination of creep and visco-inertial effects would reduce the rate below $200\,t/y$, however it was not investigated in this study. During the post-injection period, the rate for all cases drops significantly due to a rebound in the near-well temperature and the resulting reduction in the aperture of the pathway. Due to the transient nature of the temperature rebound, the rate does not reach equilibrium conditions at the end of the simulation time (5 years after the end of injection). The aquifer case on the other hand does not experience a temperature change. Therefore, that case exhibits equilibrium after the injection is ceased (Fig. $10\,$ and Fig. 12).

Fig. 15 presents the mass rate versus the final storage pressure for the depleted reservoir case. The rate shown is at the end of the simulation time (5 years after the end of injection). This is chosen as a point closest to equilibrium. According to Fig. 15, maintaining the storage pressure below 250 bar can prevent migration on the outside of the casing. CO₂ rate increases with the storage pressure. The exact level depends on the input parameters and appropriate physical mechanisms involved. The base case can be considered as the worst-case scenario estimate. However, a more likely value is between the visco-inertial and creep cases, i. e., under 500 t/y of CO₂ migration (barring the use of repair technologies that eliminate the flow). To add some context to this value, it is helpful to provide a comparison with the total stored mass of CO2. The migration rate is on a per well basis. As a thought experiment, let us assume a 50 Mt project with 5 wells in total, 3 injection wells and 2 legacy wells. The total storage amount is 10 Mt/well. We also assume that the storage complex is pressurized to the initial pressure of 274 bar and migration only occurs on the outside of the casing (all wells have competent plugs and casings). In this case, the estimated migration rate is expected to be less than 0.005 % of the stored CO2 per year, until abandonment. This rate can be reduced to zero during abandonment using leak repair technologies and competent cement plugs. Increasing the final pressure from 240 (base case) to 274 bar raises the storage capacity by approximately 14 %. This leads to an equivalent increase in the hypothetical revenue of the project based on a revenue/ton of stored CO2 model. Therefore, in some cases the economic benefit may outweigh the migration risk and should be properly evaluated.

 ${\rm CO_2}$ has a significantly higher density than methane. Therefore, buoyancy is less dominant in providing the pressure gradient necessary for upward migration. This means that a higher reservoir pressure is needed for ${\rm CO_2}$ to flow compared to methane. The minimum pressure that can cause migration depends on the downstream conditions of the pathway. In the migration pathway considered here, the flow potential

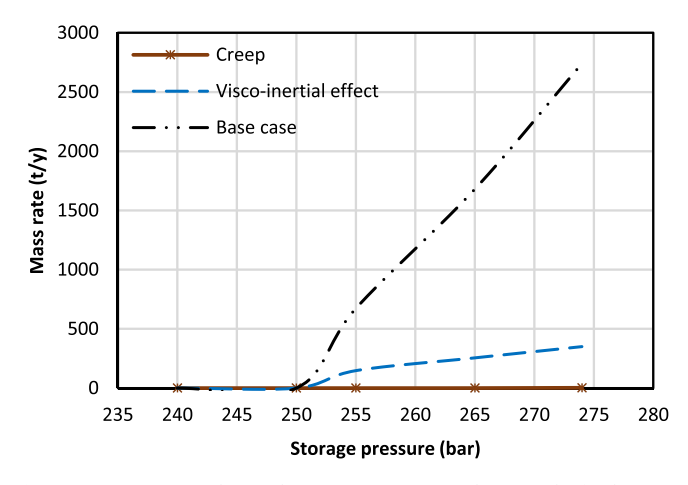


Fig. 15. CO_2 mass rate during the post-injection period, versus the final storage pressure for the depleted reservoir storage case.

of $\rm CO_2$ in the storage reservoir at 250 bar pressure exceeds the flow potential in the overburden. This is close to the hydrostatic pressure as $\rm CO_2$ density is high, in the range of 800–900 kg/m³ at the relevant pressure and temperature conditions of the case study. However, for $\rm CO_2$ or other gases at lower densities, this threshold may be lower than hydrostatic pressure. The exact value must be estimated on a case by case basis as it depends on the pressure of the overburden most likely to receive the migrating gas. A more detailed discussion on this is provided by Moghadam et al. 31

Aquifer storage case

Fig. 16 compares the migration rate for the base case, creep, and visco-inertial flow condition for the aquifer storage case. The equilibrium rate for the visco-inertial case is 300 t/y compared to 2000 t/y for the base case. The creep case indicates a mass rate of only 2-5 t/y in comparison. A storage pressure of 550 bar is assumed for all three cases.

Fig. 17 presents the equilibrium migration rate versus the storage pressure for the aquifer storage case study. The results show an increase in the mass rate as the storage pressure increases. The increase is nonlinear as the pressure changes the size of the MA as well as the pressure gradient. Compared to the depleted reservoir case, the aquifer storage case exhibits migration at early times as the pressure of the system is always above hydrostatic. Similar to the depleted reservoir case, visco-inertial effects and creep reduce the mass rate significantly. While visco-inertial effects can reduce the rate, caprock creep may halt fluid migration altogether and allow for higher injection pressures to be reached. In the absence of clear creep or non-Darcy parameters, the base case can be used as a conservative estimate of migration rate for quantitative leakage risk assessment.

It should be noted that the fluid migration rate for the two case studies in this work should not be compared as the input parameters and the assumptions are different. Particularly, the aquifer case assumes a 400 m thick caprock compared to 100 m for the depleted reservoir case. This reduces the pressure gradient at the same level of over-pressure. In addition, the size of the MA is slightly different due to different operational parameters and formation properties. Leakage assessment should be conducted on a case-by-case basis and overgeneralization should be avoided.

Self-sealing

The value of residence time is likely underestimated in Fig. 13. In the calculations, the flow is assumed to be single-phase water with dissolved CO_2 , while it is more plausible for two-phase flow conditions to exist. Therefore, the flow rate of water through the MA is overestimated, which decreases the value of the residence time. The self-sealing conditions should therefore be more favorable than the results presented

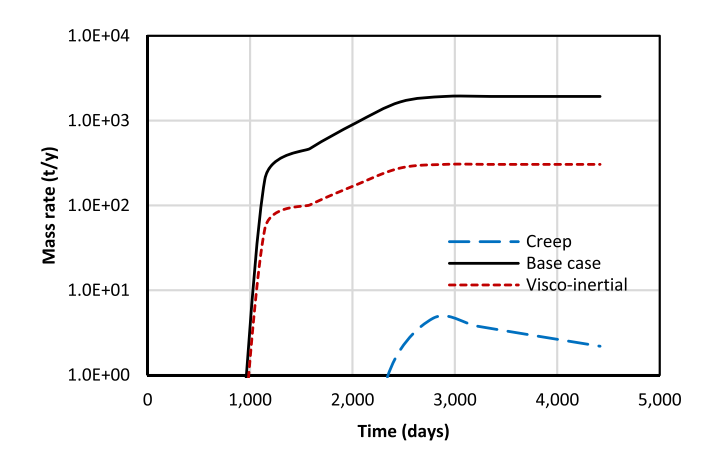


Fig. 16. Mass rate of CO_2 for the base case, creep, and visco-inertial flow for the aquifer storage base case (550 bar storage pressure).

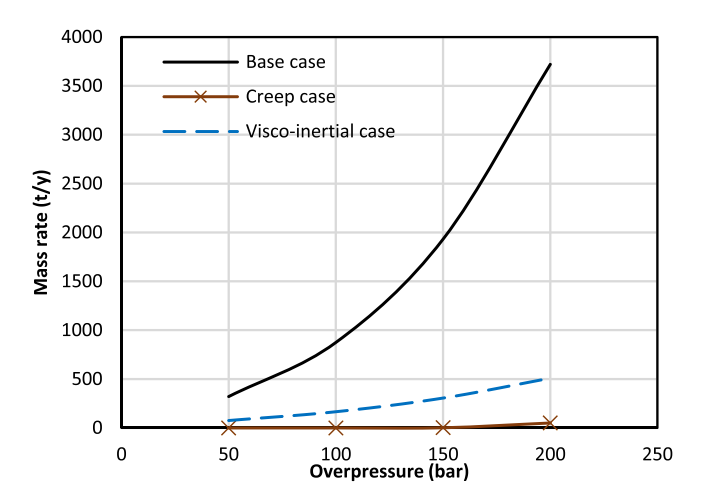


Fig. 17. Equilibrium CO₂ mass rate versus the level of overpressure in the aquifer storage case.

here. The precipitation of calcite in the lab experiments occurs within hours or days. Once CO_2 begins to flow through the MA in a dissolved state, the precipitation may gradually reduce the size of the pathway and decrease the flow rate. The decrease in the size of the pathway enhances the self-sealing conditions, further which could lead to the complete plugging of the pathway in a positive feedback loop. The effect of the gradual decline in the size of the pathway is not considered in the calculations for Fig. 13.

The self-sealing will only be possible if CO_2 dissolved in water comes into contact with cement. If the CO_2 flow along the MA is under dry conditions, calcite precipitation may not occur sufficiently to plug that path. In addition, the experimental data for self-sealing fractures over 100 micron in aperture are sparse. ⁴⁹ Therefore, more evidence of the efficacy of self-sealing process for larger defects are needed. In addition, the performance of self-sealing under field conditions is not yet verified.

Limitations

The base case/high-pressure case migration rate estimates in this study are likely overestimations. We assume single-phase gas flow in our calculations, while there is likely water in the system as well that may reduce the effective permeability of the MA to gas. In addition, the impact of formation creep and visco-inertial effects are ignored for the base case calculations that significantly impact the migration rate.

The size of the MA estimated here is the "mechanical aperture". Typically, flow is driven by "hydraulic aperture" which is smaller than the mechanical value. ^{28,29} Therefore, using hydraulic apertures would reduce the estimate of migration rate. The relationship between hydraulic and mechanical aperture for microannuli/cement fractures has been investigated experimentally. ^{28,29,2} However, more studies are needed to reach consensus in the literature. There are several other sources of uncertainty related to the magnitude of inertial effects, creep rates for different caprocks, realistic flow regimes, etc. that require lab experiments in future studies.

A relatively simple migration pathway is assumed in this work. The stored fluid is deemed to flow through the cemented annulus across the caprock and into the overburden. This implies the presence of a highly permeable overburden that can take the flow rate without a change in its pressure. In reality, the fluid may continue upwards if the overburden is not sufficiently permeable. Therefore, a more complex pathway may arise with the migrating fluid accumulating in various strata or making its way to the surface. The ultimate pathway likely depends on the relative conductivity of the various paths that are available to the fluid. Hence, permeabilities of various formations and the size of the MA along the well dictate the most likely migration pathway. In addition, fluids

may migrate through well components (packers, liner hangers, etc.), corroded casings, fractures, etc. A more holistic analysis should include the entire well envelope, stratigraphy, and physiochemical interactions. The methodology to estimate cement stress evolution was verified using lab experiments in the part I of the paper. However, Field verification of the migration rates estimation is needed to improve confidence in the model. This will be covered in future publications.

Maximum tolerable leak rate

Limiting the injection pressure below a certain threshold can prevent fluid migration through the cemented annulus. However, this comes at the cost of storage capacity. Using the methodology proposed here, the order of magnitude of unwanted fluid migration can be determined for a particular well and field (including legacy wells). Increasing the injection pressure while limiting the migration rate to a low, but non-zero value may unlock considerable storage capacity, significantly improving the economics of CCS projects. However, the definition of maximum tolerable leak rate is still lacking. This definition may be project, region, or jurisdiction specific, particularly depending on the following:

- Will the fluid migration continue long after abandonment? Fluid migration may stop due to self-sealing, formation creep, or particular abandonment operations that reduce the size of the pathway (such as milling the casing and placing cement plugs). If the flow is dramatically reduced after abandonment, then the tolerance for the leak rate during the operations may be raised.
- What is the consequence/risk of the fluid migration? A more realistic migration pathway should be modelled that includes the entire well structure and all permeable formations that are penetrated by the well. This allows for better understanding of the rate and the accumulation location of the CO₂ over time. A tolerable leak may need to have the following conditions: 1) the fluids should have a low likelihood of reaching the surface or freshwater aquifers, 2) accumulate in a formation that does not pose a hazard to any other operations/infrastructure, and 3) should remain in a small region near the well, ideally in a dissolved state.

A comprehensive risk assessment for CO_2 leakage can provide answers to such questions. ⁴⁴ In such an assessment, the impact of the calculated CO_2 leakage on people, environment, infrastructure, and climate should be considered. However, there is still a need for the relevant authorities to set an acceptable level of risk. The injection pressure of CO_2 must be set to a level that reduces the risk of damage to below the acceptable level. We argue that setting the acceptable risk level to zero is unrealistic and leads to excessively conservative project designs. This impacts the economics of projects negatively and leaves a significant portion of the storage capacity unused. The results in this study show that potential rates of leakage through MA are likely to be small. A risk assessment analysis is needed to ensure that these leakage rates pose negligible risk to people and the built environment.

Conclusions

In this two-part series, we have developed a hydro-thermomechanically coupled model to calculate potential leakage rates for CCS wells. The advantage of the present methodology is that it uses physical models (including the cement hydration process, influence of fluid pressure and temperature, visco-inertial effects, creep, etc.) to estimate the size of the flow pathway in cemented annuli. This feature leads to a methodology capable of predicting potential fluid migration rates based on the well design, formation properties, and the injection plan as opposed to purely probabilistic methods.

Two case studies were conducted focusing on an injector well in a depleted reservoir and a legacy well for an aquifer CCS project, both in

the Dutch North Sea. The results for the depleted reservoir case show that an initial microannulus during gas production may form, however, it closes as the reservoir is depleted. During CO2 injection, the microannulus gradually opens up again. Several cases were considered to investigate the impact of higher injection pressure, visco-inertial effects, and formation creep. The results show that there may be a pressure limit, below which no fluid migration occurs on the outside of the casing. Once CO₂ pressure passes this limit, flow may begin. Both case studies indicate that an increase in the final injection pressure raises the migration rate non-linearly as the higher pressure also increases the size of the microannuli. If the visco-inertial effect is considered, the rate drops significantly. Formation creep is another factor that can reduce the rate considerably. We provide a range of CO2 migration rates depending on the major mechanisms at play. The results show that fluid migration along wells through microannuli at injection pressures above hydrostatic may remain relatively small up to the initial pressure of the reservoir. Factors such as self-sealing may prevent fluid migration over time.

Quantifying the potential rate of fluid migration at various injection pressures provides the basic input for quantitative risk assessment. This analysis is crucial to avoid conservative operational conditions by setting a low target pressure for the storage complex. An increase in the final storage pressure can improve the economics of the CCS projects significantly. The ideal goal is to set a realistic target pressure while maintaining the risk and consequence of fluid migration at a reasonably low level. The analysis provided here demonstrates a workflow to conduct quantitative leakage assessment, optimize the injection strategy, maximize the use of the storage capacity, and communicate with the regulators and stakeholders. However, the model's assumptions and limitations should be further investigated in future studies. This includes the assumptions on the leakage pathway, flow models, and the mechanical behaviour of the microannuli.

CRediT authorship contribution statement

Amiri Sahar: Visualization, Methodology, Conceptualization. Moghadam Al: Writing – original draft, Visualization, Validation, Methodology, Investigation, Formal analysis, Conceptualization.

Declaration of Competing Interest

The authors declare that they have no known competing financial interests or personal relationships that could have appeared to influence the work reported in this paper

Acknowledgements

This work was supported by the RETURN project. The RETURN project is funded through the ACT programme (ACT3 Call) – Grant Number 327322, in a period from January 2022 to December 2024. We thank the following funding agencies: The Research Council of Norway (Norges forskningsråd), Netherlands Enterprise Agency (RVO), FZ Jülich PtJ (Germany), Department for Energy Security & Net Zero (UK) and Emissions Reduction Alberta (ERA, Canada). Direct financial contributions from Equinor, AkerBP, EBN, Neptune Energy Netherlands, Wintershall Dea and Harbour Energy are gratefully acknowledged. We would also like to thank Matteo Loizzo and Filip Neele for their support and feedback.

Data availability

Data will be made available on request.

References

- Agofack N, Ghabezloo S, Sulem J. Chemo-poro-elastoplastic modelling of an oilwell cement paste: macroscopic shrinkage and stress-strain behaviour. Cem Concr Res. 2020:132. 106046.
- Alberdi-Pagola P, Marcos-Meson V, Ayache AN, Fischer G. Quantitative evaluation of liquid permeability in cracked oilwell cement sheaths. SPE J. 2024;29(5): 2197–2211. https://doi.org/10.2118/218404-PA.
- Bachu S. Analysis of gas leakage occurrence along wells in Alberta, Canada, from a GHG perspective – gas migration outside well casing. Int J Greenh Gas Control. 2017; 61:146–154.
- Baumgarte C, Thiercelin M, Klaus D. Case studies of expanding cement to prevent microannular formation. Proc - SPE Annu Tech Conf Exhib, DELTA. 1999:275–282. https://doi.org/10.2523/56535-ms.
- Bell IH, Wronski J, Quoilin S, Lemort V. Pure and pseudo-pure fluid thermophysical property evaluation and the open-source thermophysical property library CoolProp. Ind Eng Chem Res. 2014;53(6):2498–2508. https://doi.org/10.1021/ie4033999.
- Bois A-P, Garnier A, Rodot F, Sain-Marc J, Aimard N. How To prevent loss of zonal isolation through a comprehensive analysis of microannulus formation. SPE Drill Complet. 2011;26(01):13–31
- Bosma, M., K. Ravi, W. van Driel, & G.J. Schreppers (1999). Design Approach to Sealant Selection for the Life of the Well. In Proceedings of the SPE Annual Technical Conference and Exhibition. 3-6 October. Houston. Texas.
- Boukhelifa L, Moroni N, James SG, Le Roy-Delage S, Thiercelin MJ, Lemaire G. Evaluation of cement systems for oil- and gas-well zonal isolation in a full-scale annular geometry. SPE-87195-PA SPE Drill Compl. 2005;20(1):44–53. https://doi. org/10.2118/87195-PA.
- Brunet J-PL, Li L, Karpyn ZT, Huerta NJ. Fracture opening or self-sealing: critical residence time as a unifying parameter for cement–CO2–brine interactions. Int J Greenh Gas Control. 2016:47:25–37.
- Carey JW. Geochemistry of wellbore integrity in CO2 sequestration: Portland cement-steel-brine-CO2 interactions. Rev Mineral Geochem. 2013;77:505–539.
- Chen YF, Zhou JQ, Hu SH, Hu R, Zhou CB. Evaluation of Forchheimer equation coefficients for non-Darcy flow in deformable rough-walled fractures. *J Hydrol*. 2015;529:993–1006. https://doi.org/10.1016/j.jhydrol.2015.09.021.
- Corina AN, Moghadam A. The sealing performance of cement sheaths under thermal cycles for low-enthalpy geothermal wells. *Energies*. 2024;17(1). https://doi.org/ 10.3390/en17010239.
- De Andrade J, Sangesland S, Skorpa R, et al. Experimental laboratory setup for visualization and quantification of cement-sheath integrity. SPE Drill Complet. 2016; 31(4):317e326.
- Fernandez SG, Matteo EN, Taha MR, et al. Characterization of wellbore microannuli. J Nat Gas Sci Eng. 2019;62:13–25. https://doi.org/10.1016/j.jngse.2018.12.003.
- Firme PALP, Brandao NB, Roehl D, Romanel C. Enhanced double-mechanism creep laws for salt rocks. Acta Geotech. 2018;13:1329–1340.
- Firme PALP, Roehl D, Romanel C. An assessment of the creep behaviour of Brazilian salt rocks using the multi-mechanism deformation model. *Acta Geotechnica*. 2016;11 (6):1445–1463. https://doi.org/10.1007/s11440-016-0451-y.
- Gasda SE, Bachu S, Celia MA. Spatial characterization of the location of potentially leaky wells penetrating a deep saline aquifer in a mature sedimentary basin. *Environ Geol.* 2004;46(6):707–720.
- Gray KE, Podnos E, Becker E. Finite-element studies of near-wellbore region during cementing operations: part I. SPE Drill Complet. 2009;24(01):127–136.
- Hatambeigi M, Anwar I, Lord DL, Hart D, Taha MR, Stormont JC. Wellbore cement fracture permeability as a function of confining stress and pore pressure. *Geomech Energy Environ*. 2023;33, 100428. https://doi.org/10.1016/j.gete.2022.100428.
- Hatambeigi M, Chojnicki K, Taha MR, Stormont JC. Visco-inertial gas flow through wellbore cement fractures. J Nat Gas Sci Eng. 2020;77(March), 103275. https://doi. org/10.1016/j.jngse.2020.103275.
- Hongjun Z, Yuanhua L, Dezhi Z, Deping Z, Feng W. Calculation analysis of sustained casing pressure in gas wells. Pet Sci. 2012;9:66–74.
- Iyer J, Walsh SDC, Hao Y, Carroll SA. Assessment of two-phase flow on the chemical alteration and sealing of leakage pathways in cemented wellbores. *Int J Greenh Gas Control*. 2018;69:72–80.
- Jackson, P.B., Murphey, C.E., 1993a. Effect of casing pressure on gas flow through a sheath of set cement. In: SPE/IADC Drilling Conference, Amsterdam, Netherlands.
- Kang M, Kanno CM, Reid MC, et al. Direct measurements of methane emissions from abandoned oil and gas wells in Pennsylvania. Proc Natl Acad Sci. 2014;111: 18173–18177.
- Laesecke A, Muzny CD. Reference correlation for the viscosity of carbon dioxide. J Phys Chem Ref Data. 2017. https://doi.org/10.1063/1.4977429.
- Lavrov A, Torsæter M. Physics and Mechanics of Primary Well Cementing. Berlin, Germany: Springer; 2016.
- Meng M, Frash LP, Carey JW, Li W, Welch NJ, Zhang W. Cement stress and microstructure evolution during curing in semi-rigid high-pressure environments. Cem Concr Res. 2021;149, 106555.
- Meng M, Frash LP, Carey JW, Mehana M, Li W, Chen B. Effect of stress-dependent microannulus aperture on well leakage. J Rock Mech Geotech Eng. 2024. https://doi. org/10.1016/j.jrmge.2024.02.004.
- Moghadam A, Castelein K, ter Heege J, Orlic B. A study on the hydraulic aperture of microannuli at the casing-cement interface using a large-scale laboratory setup. Geomech Energy Environ. 2022;29, 100269.
- Moghadam A, Loizzo M. Geomechanics for energy and the environment quantitative assessment of well leakage, part I: cement stress evolution. *Geomech Energy Environ*. 2024;40(March), 100586. https://doi.org/10.1016/j.gete.2024.100586.

- Moghadam A, Peters E, Nelskamp S. Gas leakage from abandoned wells: a case study for the Groningen field in the Netherlands. *Int J Greenh Gas Control*. 2023;126 (September 2022), 103906. https://doi.org/10.1016/j.ijggc.2023.103906.
- Nguyen P, Guthrie GD, Carey JW. Experimental validation of self-sealing in wellbore cement fractures exposed to high-pressure, CO2-saturated solutions. Int J Greenh Gas Control. 2020;100(July), 103112. https://doi.org/10.1016/j.ijggc.2020.103112.
- Nowamooz A, Lemieux JM, Molson J, Therrien R. Numerical investigation of methane and formation fluid leakage along the casing of a decommissioned shale gas well. Water Resour Res. 2015;51(6):4592–4622.
- Nygaard R, Salehi S, Weideman B, Lavoie RG. Effect of dynamic loading on wellbore leakage for the wabamun area CO2-sequestration project. J Can Pet Technol. 2014;53 (01):60-82
- Postma TJW, Bandilla KW, Celia MA. Estimates of CO2 leakage along abandoned wells constrained by new data. Int J Greenh Gas Control. 2019;84:164–179.
- Rezaeyan A, Beckie RD, Cahill AG. International Journal of Greenhouse Gas Control Multiphase flow modelling of gas migration from a hypothetical integritycompromised petroleum well in the peace region of North-eastern British Columbia, Canada. Int J Greenh Gas Control. 2024;138(September), 104261. https://doi.org/ 10.1016/j.ijggc.2024.104261.
- Rice AK, McCray JE, Singha K. Methane leakage from hydrocarbon wellbores into overlying groundwater: numerical investigation of the multiphase flow processes governing migration. Water Resour Res. 2018;54:2959–2975.
- Saint-Marc, J., Garnier, A., & Bois, A.P. (2008). Initial state of stress: The key to achieving long-term cement-sheath integrity. Proceedings - SPE Annual Technical Conference and Exhibition, 6, 4321–4334.
- Schout G, Hartog N, Hassanizadeh M, Helmig R, Griffioen J. Impact of groundwater flow on methane gas migration and retention in unconsolidated aquifers. *J Contam Hydrol*, 2020;230, 103619.
- Span R, Wagner W. A new equation of state for carbon dioxide covering the fluid region from the triple point temperature to 1100 K at pressures up to 800 MPa. J Phys Chem Ref Data. 1996;25:1509–1596. https://doi.org/10.1063/1.555991.
- Stormont JC, Fernandez SG, Taha MR, Matteo EN. Gas flow through cement-casing microannuli under varying stress conditions. *Geomech Energy Environ*. 2018;13:1–13. https://doi.org/10.1016/j.gete.2017.12.001.
- Taheri SR, Pak A, Shad S, Mehrgini B, Razifar M. Investigation of rock salt layer creep and its effects on casing collapse. *Int J Min Sci Technol*. 2020;30(3):357–365. https://doi.org/10.1016/j.ijmst.2020.02.001.

- Therond E, Bois A-P, Whaley K, Murillo R. Large-scale testing and modeling for cement zonal isolation in water-injection wells. SPE Drill Complet. 2017;32(04): 290–200
- 44. Torsæter, M., Bello-Palacios, A., Borgerud, L.K., Nygård, O.-K., Frost, T.K., Hofstad, K.H., and Andrews, J.S., (2024). Evaluating Legacy Well Leakage Risk in Co2 Storage (December 18, 2024). Proceedings of the 17th Greenhouse Gas Control Technologies Conference (GHGT-17) 20-24, Available at SSRN: https://ssrn.com/abstract=5062896 or https://doi.org/10.2139/ssrn.5062896.
- van Oort E, Juenger M, Aldin M, et al. Simplifying well abandonments using shale as a barrier. SPE Drill Complet. 2022;37(04):282–294. https://doi.org/10.2118/ 199654-PA.
- Wisen J, Chesnaux R, Werring J, Wendling G, Baudron P, Barbecot F. A portrait of wellbore leakage in northeastern British Columbia, Canada. Proc Natl Acad Sci. 2020;117:913–922.
- Wolterbeek TKT, Raoof A. Meter-scale reactive transport modeling of CO2-rich fluid flow along debonded wellbore casing-cement interfaces. *Environ Sci Technol.* 2018; 52(6):3786–3795. https://doi.org/10.1021/acs.est.7b05358.
- Wolterbeek TKT, Snippe JR, Hangx SJT. Impact of humid supercritical CO2 flow and CO2 solvation-induced cement porewater expulsion on reactive self-sealing processes along wellbore microannuli. *Geoenergy Sci Eng.* 2024;235(January), 212728. https://doi.org/10.1016/j.geoen.2024.212728.
- Wolterbeek TKT, Snippe JR, Hangx SJT. Impact of humid supercritical CO2 flow and CO2 solvation-induced cement porewater expulsion on reactive self-sealing processes along wellbore microannuli. *Geoenergy Sci Eng.* 2024;235(January), 212728. https://doi.org/10.1016/j.geoen.2024.212728.
- Zeng Z, Grigg R. A criterion for non-Darcy flow in porous media. *Transp Porous Media*. 2006;63(1):57–69. https://doi.org/10.1007/s11242-005-2720-3.
- Zhang W, Eckert A. Micro-annulus generation under downhole conditions: Insights from three-dimensional staged finite element analysis of cement hardening and wellbore operations. J Rock Mech Geotech Eng. 2020;12(6):1185–1200.
- Zhang Z, Nemcik J. Fluid flow regimes and nonlinear flow characteristics in deformable rock fractures. J Hydrol. 2013;477:139–151. https://doi.org/10.1016/j. ihvdrol.2012.11.024.
- 53. Zimmerman RW, Al-Yaarubi A, Pain CC, Grattoni CA. Non-linear regimes of fluid flow in rock fractures. *Int J Rock Mech Min Sci.* 2004;41:163–169.